Assessing the Quality of an UAV-based Orthomosaic and Surface Model of a Breakwater

Maria João HENRIQUES, Ana FONSECA, Dora ROQUE, José Nuno LIMA, João MARNOTO, Portugal

Key words: UAV, mapping, coordinates, quality control, monitoring, breakwater

SUMMARY

The low price and the quality of the products derived from photographs taken by cameras mounted on unmanned aerial vehicles (UAV) turn them very attractive to be used in several situations, namely when the area that needs to be covered hasn't a large extension or when is necessary to have data, like coordinates of points, on a periodic basis. The monitoring of the behavior of breakwaters fall is this category of works. Usually with extensions of some hundred meters long, with only a few meters high and with long flat surfaces, breakwaters are structures with a shape very attractable to be monitored by unmanned airplanes and helicopters. The National Laboratory for Civil Engineering, from Portugal, responsible by the evaluation of new methodologies and techniques applied to the monitoring of large civil engineering structures like dams, bridges, buildings and breakwaters, has been testing the use of an unmanned small airplane in the monitoring of a 400 m long breakwater. The first stage of the work was to assess the quality of the surface model built with the use of photographs taken by a small digital camera mounted on an UAV. By comparing coordinates of selected points extracted from the digital surface model, build with images taken at an average altitude of 185 m, with coordinates derived from GNSS high quality observations, it was obtained differences of 10 cm (root mean square error) in planimetry and 8 cm in height. This paper describes the conditions of the UAV flight and of the breakwater environment, conditions that were particularly hard, and presents the results of the quality control of the surface model, made with the use of statistical methods.

Assessing the Quality of an UAV-based Orthomosaic and Surface Model of a Breakwater

Maria João HENRIQUES, Ana FONSECA, Dora ROQUE, José Nuno LIMA, João MARNOTO, Portugal

1. INTRODUCTION

The breakwaters are built to protect infrastructure of ports. They are conceived and designed to withstand the most adverse and extreme weather conditions. The sea waves, the tides, the currents, the winds, the dynamics of underwater sediments, the activities of the port, are some of the factors that lead to the degradation of breakwaters, and may restrict the activity of the port. One of the most insidious degradation is the removal of support materials that takes place beneath the blocks of protection on the surface. Quite often is a localized process with slow progression, with small effects on the surface of the breakwater, but that can be responsible by a major failure of a stretch of the structure and the reduction of the functionality of the port.

When compared with structures like dams, bridges or large buildings, breakwaters are the structures much less monitored. As the deterioration of breakwaters usually doesn't put lives in danger and usually large structural modifications are a consequence of big storms that hit coastal areas, very few breakwaters are regularly monitored.

The monitoring of a breakwater, particularly the measurement of displacements, faces big challenges that have, in many cases, weak solutions. Marujo et al. (2013) has made a survey of the different monitoring techniques (expert judgment techniques and quantitative/ automated techniques) available to monitor maritime and coastal structures. These include visual inspections (walking, waterborne, airborne, diving), close-up photography (terrestrial, waterborne, aerial and airborne), photogrammetry, videogrammetry, aerial photography (with normal or with unmanned aerial vehicles (UAV)) , "crane and ball" survey, topographic survey techniques (traditional and GNSS), multibeam and side scan sonar, Lidar, satellite images, InSAR methods, laser scanning.

Especially in breakwaters that protect small ports which don't generate large income, the monitoring displacements with aerial photography taken by a digital camera mounted on an UAV should be tested because, as being a technique not too much expensive, it can represent an interesting alternative to other methods. This paper describes the first stage of a test, which is undergone, on the use of UAV techniques to monitor the displacements of the breakwater of Ericeira, a structure very exposed to the north-west Atlantic waves. Since the rebuilt in the 2010's, this breakwater has been used to test new methodologies of monitoring like the use of 3D laser, multibeam techniques and UAV-based generation of surface model. This last one is the object of the studies performed by the authors of this paper, paper that deals with the assessment of the quality of an orthomosaic and of the surface model based in photos taken from an UAV, during a flight that faced difficult conditions, also reported in this paper.

2. THE BREAKWATER OF ERICEIRA

Ericeira is a seaside resort, 35 km northwest of Lisbon, the capital of Portugal, where fishing continues to play an important role in the local economy. In the last years Ericeira area has seen growing its importance as a leisure resort due to the large number of quality surf breaks, seven, in just 4 km of coastline.

The port of Ericeira is mostly used by the local fisherman community. The advanced deterioration of the original protection of the quay (built on the 1970's) was a consequence of the effect of the highly energetic north-westerly Atlantic Ocean waves on a underdimensioned breakwater. A comprehensive study made by the National Laboratory for Civil Engineering (LNEC) in the 2000's focused on the analysis of the status of pier under the perspective of its reconstruction and development of the port. The first stage of rehabilitation is already completed (Figures 1 and 2) and focused on rebuilding the breakwater and constructing new areas and buildings to support fishing activity.

Figure 1 – Reconstruction of the breakwater of the port of Ericeira.

Figure 2 – Breakwater of the port of Ericeira after the rehabilitation.

The new rubble mound breakwater (RMB), longer and much stronger, has created a wider area of waters sufficiently calm to allow safe operations of berthing, cargo transfer, vessels manoeuvre and the protection of port infrastructures. The breakwater is 440 m long and 35 m wide. It consists of two straight lengths, angled of 147º to each other. The crest is 6.5 m wide and has an altitude of 9 m (referred to the hydrographic zero). The main elements of this breakwater are a core of finer material covered by big blocks (armor layer). Beneath the armor layer it was placed a filter layer, called underlayer, to prevent the finer material of being washed out through the armor layer.

Along the entire crest and on half of the leeside are two superstructures in concrete, being that the lowest one includes a quay. The most exposed slope of the breakwater (facing the northwesterly waves) is covered with tetrapods; the southwest extremity, which has on the top a small lighthouse, is covered with grooved cubes; the remaining areas are covered with large stones.

3. THE UAV FLIGHT

The flight of the UAV airplane was done on the 9th of February 2013, after being delayed one day because there were strong winds on the area. It had to be done during the high tide, not the best period of the day since many blocks were covered with water. The mix of these conditions (strong waves, wind, and high tide) made impossible to find a good take-off/landing area nearby the breakwater. Ericeira village, on the top of the cliff that surrounds the port (see Figure 1), with a tight urban fabric, has no good areas either. The best one, a flat field with ground vegetation and no trees or bushes, was in the surroundings of Ericeira, nearly 1200 m away from the port. Is necessary to refer that this area was also chosen because there was a clear sight to the area where the plane was going to fly. On the slope between the take-off field (with at an elevation of about 100 m) and the port there are several high buildings. For security reason the altitude of the flight could not be set to a low value.

The photos were taken by a digital camera Canon IXUS 220 HS (3000×4000 pixels), mounted on the platform SenseFly Swinglet CAM (Figure 3), a very light (500 g) and small (80 cm wingspan) plane. The emission of data like battery level, speed of the wind, position of the UAV, a transmission that was made every 0.25 s to a control unit on land, would allow the monitoring of the flight.. The control unit consists of the software eMotion (from Sensefly), installed on a laptop, this one with an external radio antenna for communication. A more comprehensive description of the system can be found in Vallet et al.(2011).

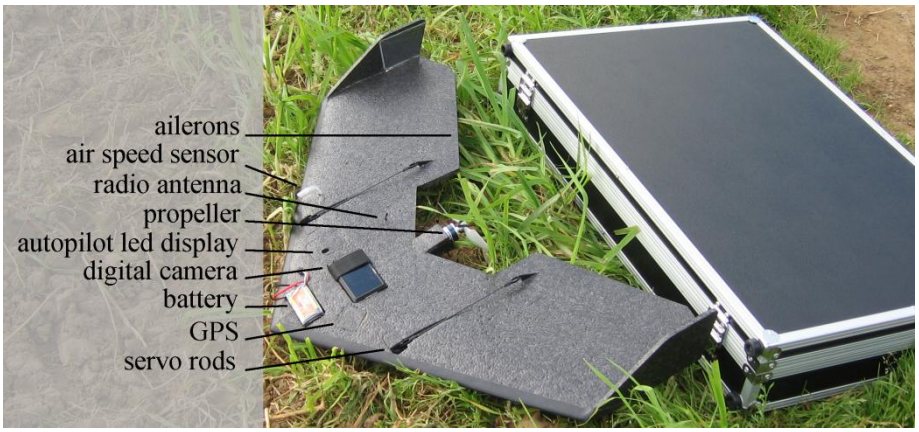

Figure 3 - Swinglet CAM and carrying case

EMotion was also used to programme the flight: to set the route, to establish the height of the flight above the ground, and to choose the points/area where to trigger the photos. In the flight above Ericeira breakwater it was set: i) the ground resolution, of 2 cm by pixel, ii) the area that needed to be covered, on a satellite view of the area downloaded from the internet, and iii) the lateral overlap of the photos of 60%, iv) the longitudinal overlap of 90%. With this information the software established automatically the flight eight (85 m), path (in the form of waypoints) and time interval between photos (a photo every two seconds). The flight plan was

done at the office and transmitted to the airplane just before the flight. As explained before, it was impossible to find a good take-off area near the breakwater being that the location chosen had a height of 100 m. For this reason the flight over the breakwater was done at an altitude of 185 m. As there is a strong connection between ground resolution and quality (Küng et al., 2011), the orthomosaic and the digital surface model generated from the photographs will have lower accuracy than initially expected.

During the flight there were problems with the transmission of data so the ground station received very few records from the airplane. When this was over the breakwater the ground station only received about 2% of the data expected, data that would have allowed to estimate the location of the airplane (latitude, longitude, altitude), its attitude, speed, etc.

But, despite the communication problems and because the plane is completely autonomous, the flight was completed. The origin of these problems of communication might be related with radio interference caused by nearby communications antennae[1]. In Figure 4 we draw on a photo the programmed path of the flight where the photos should had been taken (cyan lines) and the planimetric location of the center of photographs (yellow dots), as received at the control station. From the 75 photographs taken, the ground station only received information about the flight in three of these. In Figure 5 is presented one of the photos taken.

Figure 4 – Flight path over Ericeira breakwater.

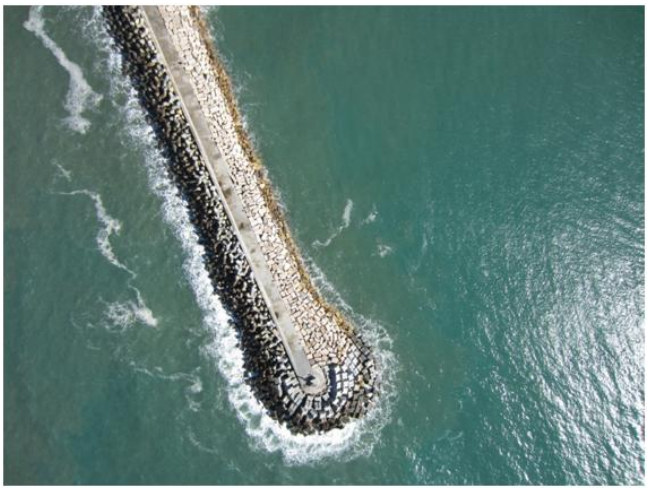

Figure 5 – Photo over the breakwater

Despite the bad conditions of the flight - the airplane flew at a higher altitude than the programmed and with high northeast winds - we got a good coverage of the breakwater, as seen in Figure 6 where we represented, over the orthomosaic of the breakwater, the approximate span of each photo on the ground (on this study it was only considered the breakwater area).

When the first group of photos were taken the airplane was flying in the SW direction, the wind was lateral from NW (see polygons delimited by a black line). The next strip, blue

[1] Just before the flight over the breakwater it was performed another flight, 3 km southeast Ericeira, over a valley only with agricultural use. In this flight the only communication problems occurred when the airplane was behind hills and there was no line of sight to it.

polygons, the airplane flew against the wind in the NE direction (its velocity slowed down and it took more photos). The wind was not constant, either in direction and velocity and the first strip was the most affected. Each spot of the breakwater was covered by at least five photos being that some features are identified in 21 photos (see example in Figure 7 of a feature that can be seen in 20 photos).

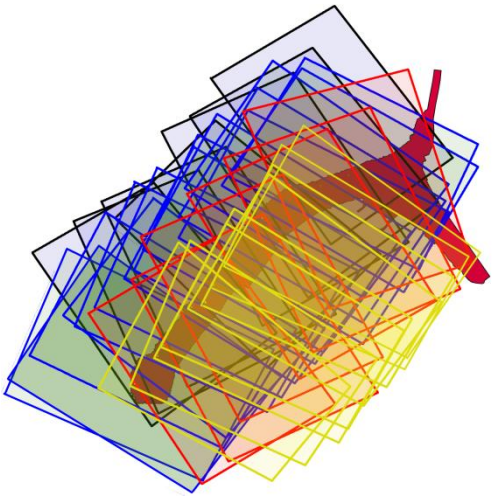

Figure 6 – Span of the photos over the breakwater

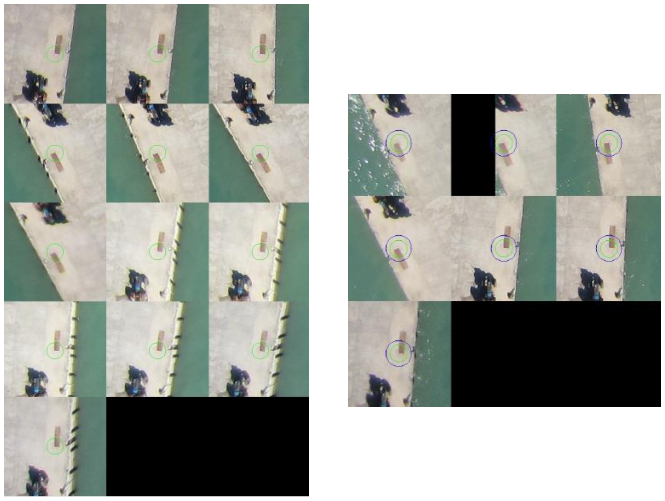

Figure 7 – Automatic identification of a feature on 20 photos

We determined the coordinates of several points (ground control points) of the superstructure of breakwater (Figure 11) by GNSS to reference the orthomosaic and the surface model and to assess planimetric and altimetric positional quality. We chose points that could be easily identified on the images (Figure 8), like the corners of the several square manhole covers placed along the superstructure (Figure 9) or the corners of the concrete base of the lighthouse (Figure 10). The points were coordinated using two Topcon choke ring antennae: one was placed on a tripod on the breakwater (reference station) and remained there during the surveying; the other was placed on the top of a stick and was placed on each point for three minutes. GNSS data was recorded at a period of 1 second. We calculated geodetic coordinates, in the ETRS89 reference frame, and cartographic coordinates, in the national coordinate system PT-TM06, using the software Pinacle and GNSS data of the nearest station of the Portuguese CORS Network.

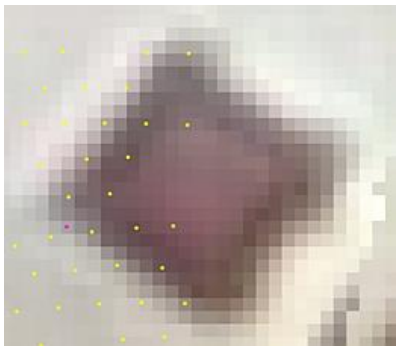

Figure 8 – Manhole as seen on a photo. On the left side yellow points of the point cloud.

Figure 9 – Southwest corner of a manhole being coordinated.

Figure 10 – Coordinating a point near the lighthouse.

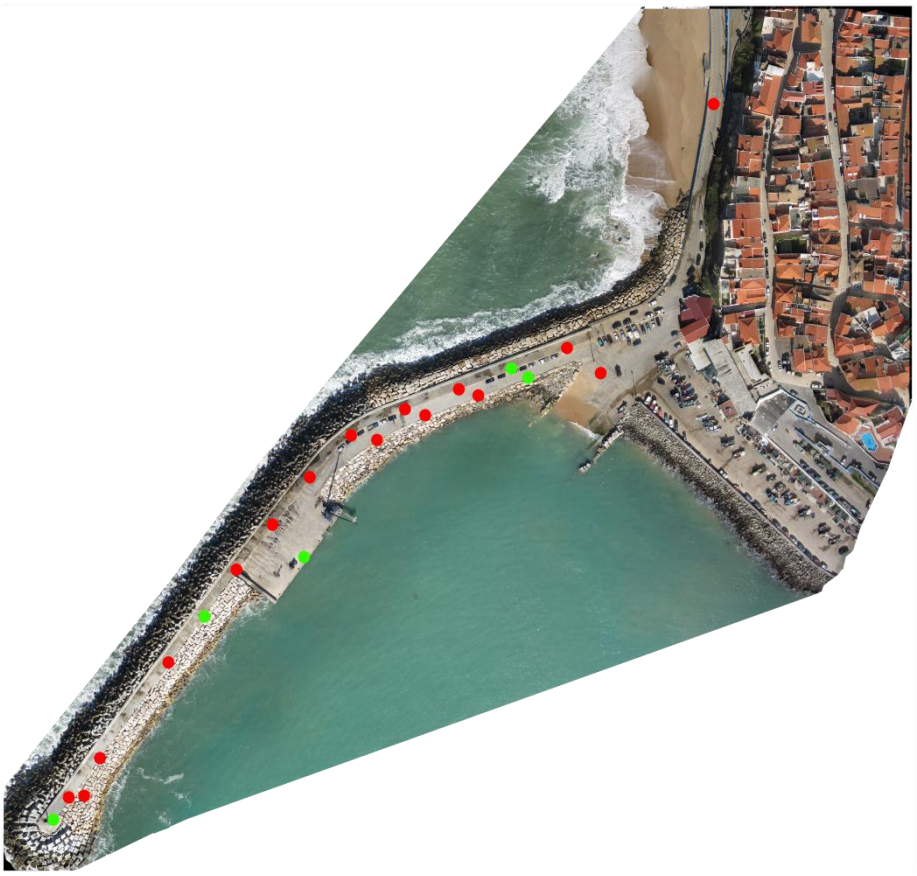

Figure 11 – Orthomosaic. Location of the ground control points.

4. DATA PROCESSING

Despite the lack of information about the flight, the processing software PostFlight Terra 3D V1, also from Sensefly, was able to produce the orthomosaic and the digital surface model.

The orthomosaic (Figure 11) is an orthogonal projection of the ground from which it is possibly to get, only, planimetric coordinates. It is the result of the combination of two photogrammetric processing tools: the ortho-rectification (correcting imagery for distortion induced by elevation using elevation data and camera model information) and the mosaicking (process of taking two or more separate images and "stitching" them together into a single image). To have information about height is necessary to build the digital surface model, which was derived from a point cloud generated also by the same software. The surface is described by a set of discrete points, independent of each other. Each one has only three attributes: the three coordinates. In Figure 12 we present the point cloud (perspective of the breakwater) where we assigned a color to each point based on its altitude. In this phase we generated, from the point cloud, a mesh composed of triangles for visualization purposes (Figure 13).

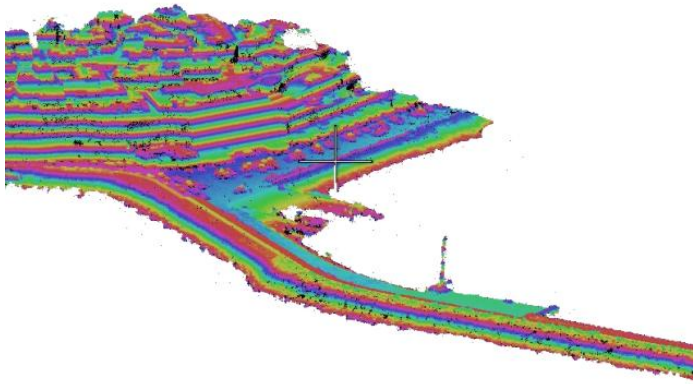

Figure 12 – Point cloud. Colors of the points related with their altitude.

Both products, generated only with very little data available from the flight, had large errors (almost 116 m in planimetry, in the south extremity of the breakwater) so we had to use some of the points coordinated by GNSS to georeference the breakwater. We chose five points (green dots in Figure 11): one point near land, other near the end of the breakwater, two in the middle.

Such a large difference, so unusual in UAV orthomosaics, are the result of: i) lack of information about the majority of the photos (coordinates of the centre of projection of the photos and airplane orientation); ii) the majority of the photos had large areas with water (water can't be used to stitch photos because is impossible to find tie points); iii) small areas with tie points: the breakwater is a long and narrow structure, that occupies a small area in each photo (photo in Figure 5 is a good example); iv) long areas with similar elements (monotonous tetrapods and stone blocks along a concrete strip). To surpass the problem the only way was, as explained, to use some of the points coordinated by GNSS as reference points. The points that we didn't use as reference points were used to assess the quality of the orthomosaic and of the surface model. In the next paragraph it will be presented the tests that will be applied and in the following paragraph the data used and the results of the tests.

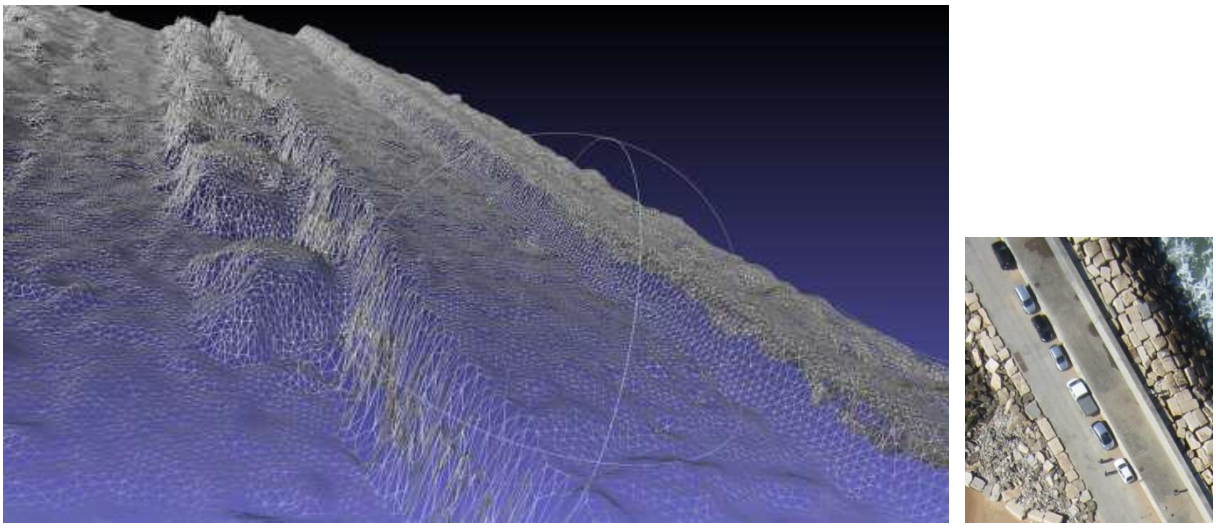

Figure 13 – Meshed surface that fits the point cloud (left image): it can be seen the lower level of the superstructure with several cars on it, parked by a vertical wall. On the right an extract of one photo, taken over the same area.

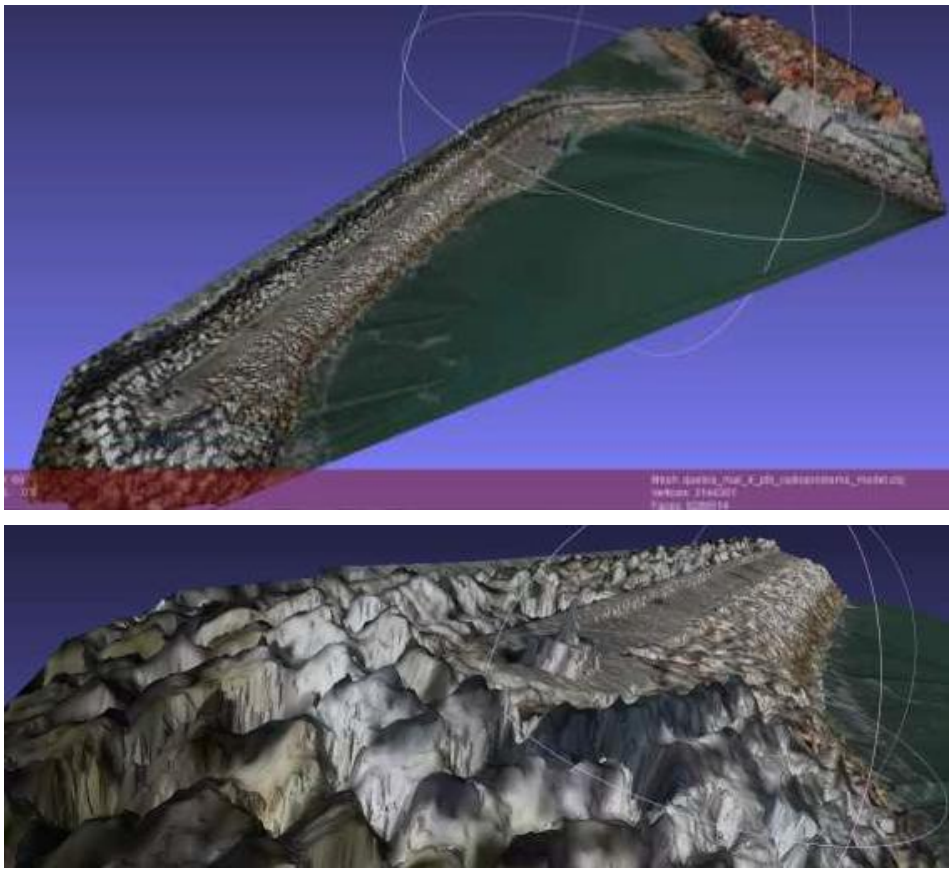

Figure 15 – Orthomosaic on the surface model.

5. STATISTICS TO TEST THE DIFFERENCES OF COORDINATES

We assessed the quality of the orthomosaic and surface model by applying statistical tests to the accuracy and the precision of the data, tests that are usually used to evaluate the positional quality (Casaca 1999, Morrison 1990). The data are differences between GNSS and photogrammetric coordinates of the ground control points. The GNSS coordinates, estimated with an error smaller than 1 cm, are more accurate than the photogrammetric coordinates obtained from the orthomosaic (2D:XY) and the surface model (1D:H), and therefore will be considered as reference coordinates.

Let H(1,n), XY(2,n) and XYH (3,n) be matrices of the differences Δ between photogrammetric and GNSS coordinates:

$$H = [\Delta h_1 \quad \Delta h_2 \quad \cdots \quad \Delta h_n] \qquad (1)$$

$$XY = \begin{bmatrix} \Delta x_1 & \Delta x_2 & \cdots & \Delta x_n \\ \Delta y_1 & \Delta y_2 & \cdots & \Delta y_n \end{bmatrix} \qquad (2)$$

$$XYH = \begin{bmatrix} \Delta x_1 & \Delta x_2 & \cdots & \Delta x_n \\ \Delta y_1 & \Delta y_2 & \cdots & \Delta y_n \\ \Delta h_1 & \Delta h_2 & \cdots & \Delta h_n \end{bmatrix} \qquad (3)$$

where n is the number of points, which can't be small.

The empirical average (scalar and vector) of the samples are determined by

$$m_H = \frac{1}{n} \sum_{i=1}^{n} \Delta h_i \qquad (4)$$

$$\vec{m}_{XY} = \begin{bmatrix} m_X \\ m_Y \end{bmatrix} \qquad (5)$$

$$\vec{m}_{XYH} = \begin{bmatrix} m_X \\ m_Y \\ m_H \end{bmatrix} \qquad (6)$$

being that m_X and m_Y of (5) and (6) are determined from expressions equivalents to (4).

The corrected empirical variance of the samples are determined by

$$s_H^2 = \frac{1}{n-1} \sum_{i=1}^{n} (\Delta h_i - m_H)^2 \qquad (7)$$

$$S_{XY} = \begin{bmatrix} S_X^2 & S_{XY} \\ S_{XY} & S_Y^2 \end{bmatrix} \qquad (8)$$

$$S_{XYH} = \begin{bmatrix} S_X^2 & S_{XY} & S_{XH} \\ S_{XY} & S_Y^2 & S_{YH} \\ S_{XH} & S_{YH} & S_H^2 \end{bmatrix} \qquad (9)$$

with the elements of the matrices presented in (8) and (9) determined by

$$S_X^2 = \frac{1}{n\text{-}1} \sum_{i=1}^{n} (\Delta x_i - m_X)^2 \quad \therefore \qquad (10)$$

$$S_{XY} = \frac{1}{n\text{-}1} \sum_{i=1}^{n} (\Delta x_i - m_X)(\Delta y_i - m_Y) \therefore \qquad (11)$$

The matrices R of the empirical correlation are

$$R_{XY} = \begin{bmatrix} 1 & r_{XY} \\ r_{XY} & 1 \end{bmatrix} \qquad (12)$$

$$R_{XY} = \begin{bmatrix} 1 & r_{XY} & r_{XH} \\ r_{XY} & 1 & r_{YH} \\ r_{XH} & r_{YH} & 1 \end{bmatrix} \qquad (13)$$

with

$$r_{XY} = \frac{S_{XY}}{\sqrt{S_X^2 \, S_Y^2}} \therefore \qquad (14)$$

where r is the correlation factor.

Under the hypothesis that the distribution of the differences of coordinates are normal, the statistics

$$v_H = n \frac{m_H^2}{s_H^2} \in F(1;n-1;\omega) \quad (15)$$

$$v_{XY} = \frac{n(n-2)}{2(n-1)} \vec{m}^T S^{-1} \vec{m} \in F(2;n-2;\omega) \quad (16)$$

$$v_{XYH} = \frac{n(n-3)}{3(n-1)} \vec{m}^T S^{-1} \vec{m} \in F(3;n-3;\omega) \quad (17)$$

are distributed as random variables F de Snedcor, with the parameter of non-centrality ω.

The statistic

$$u_H = (n-1) \frac{s_H^2}{\sigma_H^2} \in \chi^2(n-1;\omega) \text{ with } \omega = \frac{\mu_H^2}{\sigma_H^2} \therefore \quad (18)$$

is distributed as a random variable chi-square, with the parameter of non-centrality ω.

5.1 Testing the Accuracy

We characterize the accuracy of the photogrammetric coordinates by testing the centrality of the distribution of the positional errors of these coordinates. Under the null hypothesis (H0), the scalar v, from (15), (16) or (17) has a Snedecor's F distribution with f1 and f2 degrees of freedom; under the alternative hypothesis (HA) the scalar v has a non-central F distribution:

$$H0 \equiv v \in F(f1;f2) \quad ; \quad HA \equiv v \in F(f1;f2;\omega) \quad (19)$$

with f1=1, 2 or 3 when it is tested, respectively, altimetric, planimetric or 3D data. The degree of freedom f2 is equal to n-1. ω is a positive non-centrality parameter.

To test the null hypothesis against the alternative hypothesis, the variable of the test (v) is compared to the acceptance (RA) and critical (RC) regions:

$$RA = [0, q], \quad RC =]\, q, +\infty\, [\quad (20)$$

where q is the 0.95 quantile of the Snedecor's F distribution with f1 and f2 degrees of freedom.

5.2 Testing the Precision

We characterized the precision of the photogrammetric coordinates by testing the dispersion of the distribution of the positional errors of these coordinates. This test will allow us to assess if the orthomosaic/surface model is included in a pre-defined class of precision, class characterized by a tolerance (t_J), with a level of quality acceptable of, for instance, 0.95.

The variance σ_J^2 of each class "J" of precision is determined by the following expression

$$\sigma_J^2 = \frac{(t_J)^2}{q} \quad (21)$$

where q is the 0.95 quantile of the chi-squared distribution with 1, 2 or 3 degrees of freedom, depending on the coordinates (1D, 2D or 3D) being tested.

For instance, if it is considered three classes (J=I, II or III) with tolerances t_I=5 cm, t_{II}=10 cm; t_{III} = 15cm, the values of variances of each class when testing planimetric coordinates, would be σ_I^2=4.17 cm^2, σ_{II}^2=16.69 cm^2, σ_{III}^2=37.56 cm^2, since q=5.99

In this test each component, X, Y and H are analysed in an independent way. Under the null hypothesis, the scalar u, from (18) has a chi-squared distribution with (n-1) degrees of freedom; under the alternative hypothesis, u has a non-central chi-squared distribution:

$$H0 \equiv u \in \chi^2\ (n\text{-}1); \quad HA \equiv u \in \chi^2\ (n\text{-}1;\omega) \tag{22}$$

where ω is a positive non-centrality parameter. In equation (18) σ_H^2 will be replaced by σ_J^2, from the expression (21). The test will be performed as many times as the number of classes of precision established.

To test the null hypothesis against the alternative hypothesis, the variable of the test (u) is compared to the acceptance (RA) and critical (RC) regions:

$$RA = [0, q], \quad RC =]\ q, +\infty\ [\tag{23}$$

where q is the 0.95 quantile of the qui-squared distribution with (n-1) degrees of freedom.

The test just presented analyses if each component, *per se*, is included in chosen a class of precision. To perform an analysis of the planimetric coordinates together (X and Y, as a whole) it will be used a methodology adapted from the one presented by Mailing (1989). It will use a comparison of the ellipses with equal density of probability of the distribution of the planimetric inconsistencies with the corresponding circles of the planimetric tolerance. This test can be adapted to test the 3D coordinates.

Let λ be the smallest eigenvalue of the matrix of variance-covariance Σ^{-1}, matrix which is unknown. The condition

$$\frac{1}{\lambda} \leq \sigma_J^2 \tag{24}$$

is necessary and sufficient for, given a probability level (1-α), the corresponding ellipse with equal probability density lies inside the circle of tolerance with radius:

$$t_J = \sqrt{q}\ \sigma_J \tag{25}$$

where q is the probability quantile (1 - α) of a central chi-square distribution. It has two degrees of freedom when testing planimetric coordinates; three when testing 3D coordinates. Usually α=0.05.

According to Morrison (1990), the largest and the smallest eigenvalues of the matrix S^{-1} in the planimetric case (2×2 matrix) are

$$L_{max} = \frac{S_X^2 + S_Y^2 + \sqrt{\left(S_X^2 - S_Y^2\right)^2 + 4\,(S_{XY})^2}}{2\,[S_X^2\,S_Y^2 - (S_{XY})^2]} \tag{26}$$

$$L_{min} = \frac{S_X^2 + S_Y^2 - \sqrt{\left(S_X^2 - S_Y^2\right)^2 + 4\,(S_{XY})^2}}{2\,[S_X^2\,S_Y^2 - (S_{XY})^2]} \tag{27}$$

Knowing these eigenvalues is possible to build λ_*, an estimator of the smallest (λ) eigenvalue of the matrix Σ^{-1} and calculate the statistics w and the maximum likelihood estimator $\hat{\lambda}_0$ of λ.

$$\lambda_* = L_{min}\left[1 - \frac{L_{max}}{(n-1)(L_{min}-L_{max})}\right] \quad (28) \qquad w = \frac{\sqrt{n-1}}{L_{min}} \quad (29) \qquad \hat{\lambda}_0 = \frac{\sqrt{n-1}+\sqrt{n+7}}{2\,\hat{w}} \quad (30)$$

The estimates $\hat{L}_{min}$ (27), $\hat{\lambda}_*$ (28) and $\hat{\lambda}_0$ (30)) of the smallest eigenvalue λ can be used in the equation (24) to analyse if the level of tolerance can be accepted.

6. RESULTS OF APPLYING THE TESTS ON THE DATA

Ten points were used to assess the quality of the orthomosaic and the surface model. The planimetric coordinates were obtained from the orthomosaic using the software ArcGIS: the points were identified on the image and marked by a point. The attribute "planimetric coordinate" of these points were transferred automatically to a text file. The height of these points were interpolated from the 2D barycentric coordinates. The differences between photogrammetric "UAV" and GNSS coordinates are presented in Table 1.

Table 1 – Differences, in centimetres, between coordinates "UAV" (from the orthomosaic and the surface model) and coordinates GNSS.

name	ΔX	ΔY	ΔH	name	ΔX	ΔY	ΔH	name	ΔX	ΔY	ΔH	name	ΔX	ΔY	ΔH
P1	-3.1	-3.8	-1.6	P5	1.1	-5.1	4.2	P16	1.7	-4.0	-4.3	Q44	-0.4	-10.3	7.4
P2	0.8	-3.6	6.4	P7	-2.8	-2.6	17.3	P18	-4.4	1.1	1.0	Q48	-2.4	-12.8	4.9
P3	3.1	-1.3	1.6	P9	-3.9	-7.8	11.3	P20	0.5	-13.8	1.9	Q49	8.6	-6.0	1.9
P4	0.1	0.2	1.3	P10	4.3	-14.0	15.4	Q10	12.3	-10.7	4.3	Q81	8.9	-9.1	14.0

The next step of the evaluation is to determine the empirical averages and variances (see values in Table 2).

Table 2 – Empirical averages (m) and variances (S^2)

m_H= 5.4 cm	m_X = 1.5 cm	m_Y=-6.5 cm	(4)
SH2= 38.4 cm^2	$S_{XY}=\begin{bmatrix}23.9 & -7.6\\ -7.6 & 24.0\end{bmatrix}$ cm^2	$S_{XYH}=\begin{bmatrix}23.9 & -7.6 & 2.0\\ -7.6 & 24.0 & -10.5\\ 2.0 & -10.5 & 38.4\end{bmatrix}$ cm^2	(7) to (11)
	r_{XY}=-0.32	r_{XY}=-0.32, r_{XH}=-0.06, r_{YH}=-0.35	(12) to (14)

With these values we were able to perform the calculus of: i) statistics v_H, v_{XY} and v_{XYH}, and also of the statistics v_X and v_Y (Table 3) to test the accuracy, ii) statistics u and the eigenvalues of matrices to test the precision (Tables 4 and 5).

Table 3 – Testing the accuracy

v_H=12.4; q=4.5; rejected v_X=1.6; q=4.5; accepted v_Y=27.9; q=4.5; rejected	v_{XY}=13.1; q=3.7; rejected	v_{XYH}=9.0 q=3.4; rejected	(15) to (17) and (20)

When v ≤q the distribution of the errors is central. In Table 3 it can be seen that only the positional errors of the X component have a central distribution. This is not a surprise after a simple analysis of the values of Table 1, where it can be seen that the majority of the differences of the components Y and H have the same sign.

Table 4 – Testing the precision. Each component *per se*

Class I: t_I = 5 cm	Class II: t_{II} = 10 cm	Class III: t_{III} = 15 cm	Class IV: t_{IV} = 20 cm	
u_X = 55.11 u_Y = 55.31 u_H = 88.44 q=7.26	u_X = 13.78 u_Y = 13.83 u_H = 22.11 q=7.26	u_X = 6.12 u_Y = 6.15 u_H = 9.83 q=7.26	u_X = 3.44 u_Y = 3.46 u_H = 5.53 q=7.26	(18) and (23)

According to the data presented in Table 4, the orthomosaic can be included in class III of dispersion because both statistics (u_X and u_Y) are smaller than q (the 0.95 quantile of the central chi-square distribution with 15 degrees of freedom). The component altitude, if considered independent, is classified has belonging to the class IV of dispersion.

Table 5 – Testing the precision of the planimetric and 3D coordinates.

t_I = 5 cm; σ_I^2 = 4.2 cm^2 t_{II} =10 cm; σ_{II}^2 = 16.7 cm^2 t_{III} = 15cm; σ_{III}^2 = 37.6 cm^2 t_{IV} = 20cm; σ_{III}^2 = 66.8 cm^2	t_I = 5 cm; σ_I^2 = 3.2 cm^2 t_{II} =10 cm; σ_{II}^2 = 12.8 cm^2 t_{III} = 15cm; σ_{III}^2 = 28.8 cm^2 t_{IV} = 20cm; σ_{III}^2 = 55.1 cm^2	(21)
S_{XY} $\hat{L}_{Max}$= 0.061 cm^{-2} $\hat{L}_{Min}$= 0.032 cm^{-2} ⇒ $1/\hat{L}_{Min}$=31.56 cm^2 $\hat{\lambda}_*$ = 0.036 cm^{-2} ⇒ $1/\hat{\lambda}_*$=27.72 cm^2 $\hat{\lambda}_0$ = 0.035 cm^{-2} ⇒ $1/\hat{\lambda}_0$ = 28.20 cm^2 $\sigma_{II}^2 < 1/\hat{L}_{Min}, 1/\hat{\lambda}_*, 1/\hat{\lambda}_0 < \sigma_{III}^2$	S_{XYH} $\hat{L}_{Max}$= 0.070 cm^{-2} $\hat{L}_{Min}$= 0.022 cm^{-2} ⇒ $1/\hat{L}_{Min}$=45.20 cm^2 $\hat{\lambda}_*$ = 0.024 cm^{-2} ⇒ $1/\hat{\lambda}_*$=41.18 cm^2 $\hat{\lambda}_0$ = 0.025 cm^{-2} ⇒ $1/\hat{\lambda}_0$ = 40.39 cm^2 $\sigma_{III}^2 < 1/\hat{L}_{Min}, 1/\hat{\lambda}_*, 1/\hat{\lambda}_0 < \sigma_{IV}^2$	(27) to (30) and (24)

To determine the eigenvalues of the matrix S_{XYH} it was used the Excel addin Matrix.

To set the class of dispersion of the planimetric coordinates and of the 3D coordinates, it were used the three estimators of λ, presented in the end of the last paragraph. In the last line of Table 5 are presented the values calculated for these three estimators. According to these and the classes chosen, the orthomosaic belongs to the class III of tolerance; the surface model (that gathers planimetric coordinates with altitude) belongs to the class IV of dispersion.

7. CONCLUSIONS

It was presented several tests that can be used to assess the positional quality in products used to represent the surface of the Earth. It was applied to analyse the quality of an orthomosaic and a surface model produced from photos of a breakwater. The photos were taken by a common digital camera mounted on a UAV airplane. The flight was done under bad conditions: strong wind, unknown position and attitude of the airplane due to the lack of communication.

The root mean square error of the photogrammetric "UAV" coordinates is 10 cm in planimetry, 8 cm in heigh. The tests performed indicate that the accuracy was not achieved while concerning the precision the orthomosaic lies in Class III (15 cm) and the surface model in Class IV (20 cm).

These values are worse than the ones obtained from a very recent flight made with the same equipment over an area of 13.2 ha (the breakwater flight covered an area of 9.5 ha). In this larger area, in a city, it was possible to choose reference and control points all over it. There, we were not limited to a narrow strip as in the breakwater study. Maybe this was the main reason for the achievement of better results.

REFERENCES

Casaca,J. 1999. A Avaliação da Qualidade Posicional de Cartografia Topográfica em Escalas Grandes. Atas da II Conferência Nacional de Cartografia e Geodesia.

Küng, O., Strecha, C., Beyeler, A., Zufferey, J.-C., Floreano, D., Fua, P., and Gervaix, F.:2011. The accuracy of automatic photogrammetric techniques on ultra-light UAV imagery, Int. Arch. Photogramm. Remote Sens. Spatial Inf. Sci., XXXVIII-1/C22, 125-130, doi:10.5194/isprsarchives-XXXVIII-1-C22-125-2011.

Mailing, D. 1989. Elements of Cartometry. Pergamon Press.

Marujo,N.; Trigo-Teixeira,A.; Sanches do Valle,A.; Araújo,M.A.; Caldeira,J. 2013. An improved and integrated monitoring methodology for rubble mound breakwaters – application to the Ericeira breakwater. 6th SCACR – International Conference on Applied Coastal Research.

Morrison,D. 1990. Multivariate Statistical Methods. McGraw-Hill.

Vallet, J., Panissod, F., Strecha, C., and Tracol, M. 2011. Photogrammetric performance of an ultra light weight swinglet "UAV", Int. Arch. Photogramm. Remote Sens. Spatial Inf. Sci., XXXVIII-1/C22, 253-258, doi:10.5194/isprsarchives-XXXVIII-1-C22-253-2011.

BIOGRAPHICAL NOTES

Maria João Henriques is a Senior Research Officer at the Applied Geodesy Division of LNEC. Her research activities include geodetic surveying systems design and quality control, atmospheric effects on the measurements, calibration of equipment.
Ana Fonseca is a Senior Research Officer at the Applied Geodesy Division of LNEC, with a PhD on Remote Sensing. Her research activities includes Remote Sensing, Photogrammetry and Digital Image Processing applied to urban planning, risk prevention and infrastructure monitoring.
Dora Roque is a Grant Holder at the Applied Geodesy Division of LNEC. Her areas of interest include Remote Sensing, Photogrammetry and Digital Image Processing.
José Nuno Lima is a Research Officer at the Applied Geodesy Division of LNEC. His areas of research include Geodesy, GNSS, the monitoring of civil engineering structures, time series analysing and filter design.
João Marnoto is the director of the Geospatial Services unit of SINFIC. His activities include consultancy in projects of designing of solutions GIS, definition of geographic data models and database design, control and quality assessment of cartographic information.

CONTACTS

Maria João Henriques	Ana Fonseca	Dora Roque	José Nuno Lima
Tel. +351 218443396	+351 218443779	+351 218443531	+351 218443409
mjoao@lnec.pt	anafonseca@lnec.pt	droque@lnec.pt	jnplima@lnec.pt

Laboratório Nacional de Engenharia Civil
Av. Brasil 101
1700-066 Lisbon, PORTUGAL
www.lnec.pt

João Marnoto
SINFIC
Estrada da Ponte, nº2
Quinta Grande - Alfragide
2610-141 Amadora, PORTUGAL
Tel. +351 210103900
jmarnoto@sinfic.pt
www.sinfic.pt